Bone histology of the non-iguanodontian ornithopod *Jeholosaurus shangyuanensis* and its implications for dinosaur skeletochronology and development

Fenglu Han , Qi Zhao , Josef Stiegler & Xing Xu

View supplementary material

Published online: 12 Aug 2020.

Submit your article to this journal

View related articles

View Crossmark data

Check for updates

ARTICLE

BONE HISTOLOGY OF THE NON-IGUANODONTIAN ORNITHOPOD *JEHOLOSAURUS SHANGYUANENSIS* AND ITS IMPLICATIONS FOR DINOSAUR SKELETOCHRONOLOGY AND DEVELOPMENT

FENGLU HAN,[*,1,2] QI ZHAO,[2] JOSEF STIEGLER,[†,3] and XING XU[2]
[1]School of Earth Sciences, China University of Geosciences (Wuhan), No. 388 Lumo Road, Wuhan 430074, China, hanfl@cug.edu.cn;
[2]Key Laboratory of Evolutionary Systematics of Vertebrates, Institute of Vertebrate Paleontology and Paleoanthropology, Chinese Academy of Sciences, 142 Xizhimenwai Street, Beijing 100044, China, zhaoqi@ivpp.ac.cn, xu.xing@ivpp.ac.cn;
[3]Department of Biological Sciences, George Washington University, 2029 G Street, NW, Washington, D.C., 20052, U.S.A., josef.stiegler@stonybrook.edu

ABSTRACT—Bone histology has provided valuable information on the life history of dinosaurs, and the presence of growth lines provides useful information for age estimation, growth variation, and the reconstruction of paleobehavior. Here, we present new data recovered from five individuals of the non-iguanodontian ornithopod dinosaur *Jeholosaurus shangyuanensis* from the Early Cretaceous Jehol Biota. These specimens, ranging in body length from 16 to 62 cm, represent early juvenile, late juvenile, and subadult ontogenetic stages. The bones of *Jeholosaurus* mainly consist of fibrolamellar tissue, which is similar to that of other non-iguanodontian ornithopods; however, parallel-fibered bone and lamellar bone tissues were also deposited in early juvenile through subadult individuals, suggesting relatively slow growth rates. Parallel-fibered bone is only regionally present in the juvenile but is well developed throughout the outermost cortex of the subadult. Skeletochronology indicates that these specimens range in age from one to five years old. Analyzing bone tissue distribution and lines of arrested growth (LAGs) in these specimens, we estimate that *Jeholosaurus* reached sexual maturity at two to four years old. The largest individual (IVPP V15939) displays an apparently higher growth rate during the first two years, which is abruptly reduced in the following years, suggesting a distinct growth pattern that may be related to sexual dimorphism or variable environmental conditions. Finally, the largest specimen displays parallel-fibered bone tissue but lacks an external fundamental system (EFS) near the periphery, suggesting that it was still growing but was approaching somatic maturity at death.

SUPPLEMENTAL DATA—Supplemental materials are available for this article for free at www.tandfonline.com/UJVP

INTRODUCTION

Bone histology has provided important information on dinosaur physiology and growth patterns, including growth rates (Erickson et al., 2001; Padian et al., 2001; Chinsamy-Turan, 2005), longevity (Erickson, 2005; Hübner, 2012), sexual maturity (Erickson et al., 2007; Lee and Werning, 2008), somatic maturity (Sander et al., 2006), metabolic rates (Grady et al., 2014), and social behavior (Zhao et al., 2014). Previous studies show that most dinosaurs grew with fibrolamellar bone tissue type that is interrupted by the formation of lines of arrested growth (LAGs). Bone tissues suggest that the growth rates of dinosaurs are faster than those of most extant reptiles (Erickson et al., 2001; Erickson, 2005). Small dinosaurs usually have moderate growth rates, whereas large species could grow as fast as large mammals (Erickson, 2005). Counting the number of LAGs is a common method for evaluating the individual longevity of dinosaurs (Castanet, 1994). However, this method does not always provide a correct age due to the remodeling and expansion of the marrow cavity (Horner et al., 1999). Several methods have been used to reconstruct the number of missing LAGs (Zug and Wynn, 1986; Klein and Sander, 2007; Lee and O'Connor, 2013; Lee et al., 2013; Woodward et al., 2013), and the most informative method is to analyze samples from an ontogenetic series of individuals (Lee and Werning, 2008; Reizner, 2010; Zhao et al., 2013).

Analyses of bone histology from the ontogenetic series of individuals are likely to provide more accurate information to address the abovementioned issues pertaining to the reconstruction of dinosaur life histories (Zhao et al., 2013). This approach has been applied to the non-neoceratopsian ceratopsian *Psittacosaurus* (Erickson and Tumanova, 2000; Erickson et al., 2009; Zhao et al., 2019), the small ornithopods *Gasparinisaura cincosaltensis* (Cerda and Chinsamy, 2012), the iguanodontians *Dryosaurus* (Horner et al., 2009), *Dysalotosaurus* (Hübner, 2012), and *Tenontosaurus* (Werning, 2012), the hadrosaurid *Maiasaura* (Horner et al., 2000; Woodward et al., 2015), as well as some sauropodomorphs (Klein and Sander, 2007, 2008) and theropods (Erickson et al., 2004; Horner and Padian, 2004; Bybee et al., 2006; Wang et al., 2017; Lee and O'Connor, 2013).

Ornithopoda represents one of the most successful ornithischian dinosaur clades, living on all continents during the Cretaceous. Early-diverging ornithopods are generally small and bipedal (sometimes referred to as 'hypsilophodontids';

*Corresponding author.
†Current address: Department of Anatomical Sciences, Stony Brook University, Stony Brook, New York 11794-8081, U.S.A.

Color versions of one or more of the figures in the article can be found online at www.tandfonline.com/ujvp.
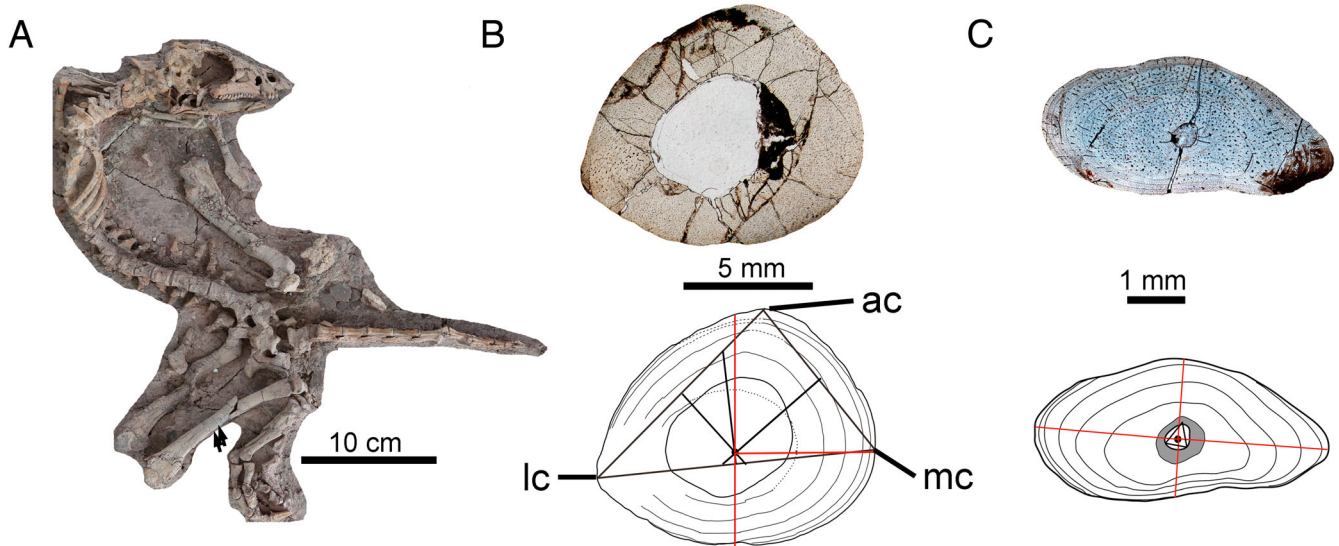
FIGURE 1. The skeleton of the smaller subadult *Jeholosaurus shangyuanensis* (IVPP V20379) and the locations of histological sampling. **A**, the whole skeleton. The black arrow indicates the sectional positions. **B**, cross-section and line drawing of LAGs in the right tibia. **C**, cross-section and line drawing of LAGs in the right fibula. Thick lines represent the border of the medullary cavity and the outline of the whole cross-section. Fine lines indicate LAGs. Fine dotted lines indicate obscured or missing portions of LAGs. Black point is the center of the extremities of each corner. Red lines are the distances from the center to each LAG and periphery. The gray areas all indicate endosteal bone layers. **Abbreviations**: **ac**, anterior corner; **lc**, lateral corner; **mc**, medial corner.

Butler et al., 2008), and the clade includes much larger quadrupedal forms during the Cretaceous (Norman et al., 2004; Butler et al., 2008). Previous studies on bone histology of the ornithopods have significantly enhanced our understanding of their physiology and behavior. The ornithopods are well known histologically in comparison with other major dinosaurian clades (Chinsamy, 1995; Horner et al., 2000, 2009; Cerda and Chinsamy, 2012; Hübner, 2012; Werning, 2012; Woodward et al., 2015). Hübner (2012) suggested that there are two types of bone tissue in ornithopods based on distinct body size: large ornithopods have well-developed growth cycles with annuli/LAGs, whereas small ornithopods have less pronounced annuli/LAGs than large ornithopods in subadult or adult individuals due to lower demand for food, no need for migration, and precocial young (Hübner, 2012). However, the well-developed LAGs and annuli present in the small ornithopod *Gasparinisaura* suggest that there is a greater diversity of growth patterns among ornithopods than has been previously suggested (Cerda and Chinsamy, 2012).

Jeholosaurus shangyuanensis is a small non-iguanodontian ornithopod from the Lower Cretaceous Yixian Formation in Liaoning Province, China (Xu et al., 2000). The skeletal morphology has been described based on well-preserved specimens (Barrett and Han, 2009; Han et al., 2012), but other aspects of this species such as growth dynamics and physiology are poorly known. Here, we examine the bone histology of *Jeholosaurus shangyuanensis* based on five individuals of different sizes (Fig. 1; Table 1) and provide growth rates, individual growth variation, and other life-history aspects of this dinosaur, which will contribute to understanding the diversity of growth strategies among non-iguanodontian ornithopods.

Institutional Abbreviations—**IVPP**, Institute of Vertebrate Paleontology and Paleoanthropology, Beijing, China; **MOR**, Museum of the Rockies, Bozeman, Montana, U.S.A.

MATERIALS AND METHODS

Five individuals of *Jeholosaurus* (IVPP V12529, IVPP V15719, IVPP V20380, IVPP V20379, and IVPP V15939) were selected for histological analysis (Table 1; Figs. 1, 2). All materials came from the Lujiatun Bed of the Yixian Formation (Lower Cretaceous) of Lujiatun, Liaoning Province, China (He et al., 2006), but may come from different stratigraphic levels within the Lujiatun Bed based on color differences in matrix associated with each individual (Han et al., 2012). The skeletal morphology of IVPP V15719, IVPP V12529, and IVPP V15939 was described in previous papers (Barrett and Han, 2009; Han et al., 2012). IVPP V20379 (Fig. 1) and IVPP V20380 preserved complete skulls and postcranial skeletons and are assignable to *Jeholosaurus shangyuanensis* based on a combination of characters. IVPP V20379 was identified as *J. shangyuanensis* based on the following characters: the presence of six premaxillary teeth, the triangular maxillary teeth without primary ridge, triangular antorbital fenestra, and fused distal tarsals 1 and 2. IVPP V20380 was assigned to be *J. shangyuanensis* by the following features: six premaxillary teeth, subtriangular maxillary tooth crowns, sharp anterior end of the predentary, the elongate ilium with a slender preacetabular process and a short and deep postacetabular process, a brevis fossa facing ventrally, and the ischial shafts appressing to each other for approximately 70% of their lengths distally. Sections were sampled from the mid-diaphyses of tibiae and fibulae because of these elements' diminished potential for remodeling relative to other long bones (Horner et al., 1999). The sampled positions are listed in Table 1. All tibiae have subtriangular cross-sections, with the distances from the proximal ends to the sampled positions among 51–55% of the entire lengths of the tibiae (Table 1), whereas the cross-sections of the fibulae are variable from subelliptical to subcircular in outline due to slightly different sectional positions (Fig. 2). The tibiae and the fibulae were sampled together in the smallest individual IVPP V15719, the holotype specimen IVPP V12529, and the largest individual IVPP V15939, and their fibulae have subcircular cross-sections. The other two individuals, IVPP V20379 and IVPP V20380, on the other hand, have more elliptical cross-sections due to more proximally positioned sections (Fig. 2).

The preparation of the histological sections was carried out at the IVPP. The selected bones were processed using the Exakt cutting-grinding system (Gotfredsen et al., 1989; Donath and

TABLE 1. Specimens of *Jeholosaurus shangyuanensis* used for histological analysis.

Specimen number	Element	Element length (mm)	Sectional position (mm)	Body length (mm)	Preserved LAGs	Age estimation (years)	Medullary area/cortex ratio	Growth stage
IVPP V15719	Right tibia	65	33	160	0	<1	0.4	Early
	Right fibula	61	31		0		0.11	juvenile
IVPP V12529	Right tibia	108	58	270e	2	2	0.21e	Late juvenile
	Right fibula	101	58		2		0.02	
IVPP V20380	Right tibia	135	73	520	3	3	0.23	Late juvenile
	Right fibula	130e	55		3		0.01	
IVPP V20379	Right tibia	127	69	440	5	5	0.20e	Subadult
	Right fibula	121e	55		5		0.01	
IVPP V15939	Right tibia	161	86	620e	5	5	0.18	Subadult
	Right fibula	148	83		5		0.007	

Sectional position is the distance from the proximal end to the positional site. e = estimated value.

Rohrer, 2003). Sections were embedded in Exakt Technovit 7200 one-component resin, cut with an Exakt-300CL automatic microtome, and ground to a thickness of about 60 μm using Exakt 400CS grinding machine with P800 and P4000 abrasive paper. The polished thin sections were then observed under transmitted and polarized light. Thin section slides were photographed using a Leica DM-RX optical microscope. Nomenclature and definitions of structures follow Francillon-Viellot et al. (1990) and Chinsamy-Turan (2005).

Some previous estimations of vascular density use qualitative terms, such as 'very dense' or 'moderately dense' canals. Here, we follow the terms of Warshaw (2008). The terms 'dense vascularization' or 'highly vascularized' are in reference to vascular canals separated from each other by less than the diameter of two canals. 'Moderately dense vascularization' was defined as the distance between vascular canals less than three times the diameter of the canals. 'Sparse vascularization' or 'poorly vascularized canals' was defined as the distance between vascular canals more than three times the diameter of the canals.

Estimations of individual age were calculated by counting LAGs in both tibiae and fibulae (Fig. 2). The LAGs that have been destroyed because of the expansion of the medullary cavity or remodeling in large individuals can be retrocalculated by the examination of small individuals. This assumes minimal variation in growth rates of the tibiae and fibulae for all the individuals. We correlated the LAGs of all cross-sections to count the final number of LAGs in each individual and assume a correspondence between years of growth and annual deposition of LAGs (Castanet et al., 1993).

In order to calculate the cortical thickness deposited for each year in each individual, we measured the distance from the centroid of the medullary cavity to each LAG by choosing a standard location within each cross-section that is unambiguous and repeatable for all cross-sections (Fig. 1). In the cross-sections of the tibiae, a triangle was drawn by connecting the extremities of each corner (including lateral, medial, and anterior; Fig. 1B), and then the centroid of this triangle was generated (Hübner, 2012). The distance between the cross-sectional centroid and each of the LAGs was measured for all cross-sections. To calculate the thickness of each growth cycle, three points at each LAG in different directions were chosen, which were taken at the same position in each individual (Fig. 1). Finally, the average distance from the centroid to each LAG was generated for all the cross-sections, and the thickness of each growth cycle would be the radial distance between successive LAGs (Fig. 1; Table S1).

In the fibulae, the calculation of cortical thickness differs from that of the tibia because the centroid is usually located outside the medullary cavity if calculated using the whole cross-section (Fig. 1C). Therefore, the centroid of a triangle was generated by connecting the extremities of the medullary cavity (not the whole cross-section). Four points at each LAG in different directions (the lines connecting the centroid and the points are perpendicular to each other) were chosen, which were taken at the same position in each individual. The distance from the centroid to each LAG was then measured. All measurements were then recorded in Excel (Microsoft Office 2013), and the correlations of growth cycles to each year were calculated for each individual (Table S2).

The ratio of medullary cavity area to that of the cortex was also calculated in both tibiae and fibulae (Table 1) using ImageJ 1.52a (Abràmoff et al., 2004). A complete cross-section of the tibia was reconstructed in IVPP V12529 based on the cross-sectional morphology of other tibiae (Fig. 2B).

RESULTS

General Histological Features

The cross-sectional shape of the tibiae is triangular in outline. It expands laterally to anterolaterally to form a wedge-shaped area near the contact and/or ligamentous connection with the fibula (Fig. 2). The tibia has a large medullary cavity and a thin, compact cortex in the smallest individual (IVPP V15719), but the compact cortices become thickened in large individuals and the medullary cavities are relatively smaller than in small individuals (Table 1). The shape of the medullary cavity is elliptical and is wider mediolaterally than anteroposteriorly. There is no endosteal layer surrounding the medullary cavity preserved in any tibia. The tibial cross-sections mainly consist of the woven-fibered bone matrix with a moderate density of well-developed primary osteons and are interrupted by the formation of LAGs and annuli (Table 2). In the zones, the vascular canals are mainly longitudinal but are often either transversely connected or with irregular and trifurcate canals, especially in large individuals. The osteocyte lacunae are abundant and randomly distributed throughout the cortex. They are more obvious in the outer and inner cortex (Fig. S1B) than in the mid-region (Fig. S1C), likely due to taphonomic processes (possibly bacterial/fungal growth). The annuli consist of lamellar bone matrix with few vascular canals and flattened osteocyte lacunae that are arranged with their long axes parallel to the LAGs. Parallel-fibered bone is present at the lateral corner adjacent to the fibula of the cross-section in all of our samples (e.g., Fig. S1D, E) and is present throughout the outer cortex of the subadult stage (IVPP V20379 and IVPP V15939). Remodeling is present but restricted to the area adjacent to the fibula in all the specimens except the smallest individual (IVPP V15719), which possesses no secondary osteons. This area has a dense network of collagen
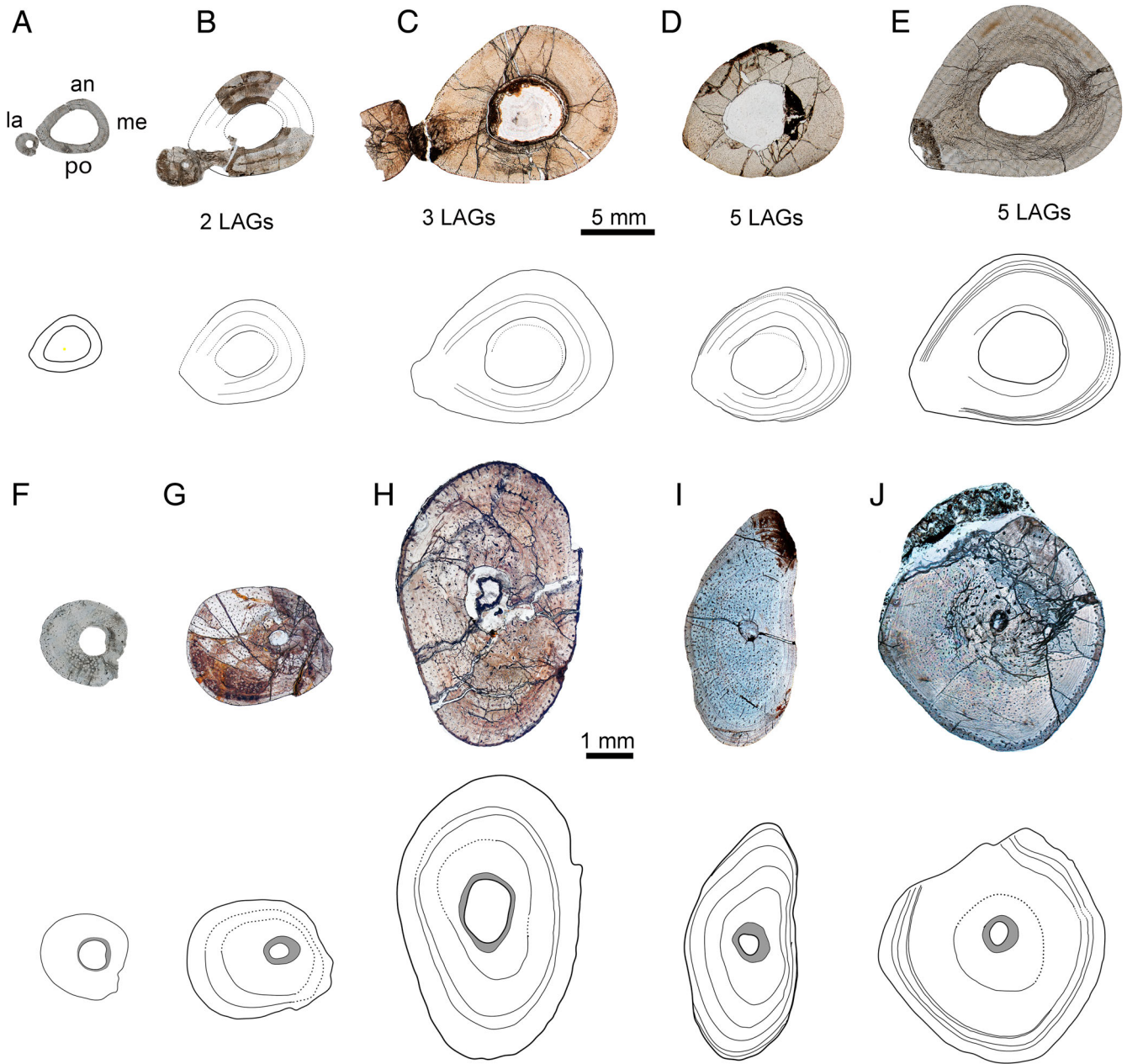
FIGURE 2. Cross-sections and line drawings of LAGs (thin lines) through tibiae and fibulae in *Jeholosaurus shangyuanensis*. **A**, IVPP V15719, tibia and fibula; **B**, IVPP V12529, tibia and fibula; **C**, IVPP V20380, tibia and partial fibula; **D**, tibia of IVPP V20379; **E**, tibia of IVPP V15939; **F**, fibula of IVPP V15719; **G**, fibula of IVPP V12529; **H**, fibula of IVPP V20380; **I**, fibula of IVPP V20379; **J**, fibula of IVPP V15939. All cross-sections are cut at or near the mid-diaphysis. Fine dotted lines indicate obscured or missing portions of LAGs. The gray areas all indicate endosteal bone layers. **Abbreviations**: **an**, anterior; **la**, lateral; **me**, medial; **po**, posterior.

fibers, is heavily remodeled by secondary osteons, and is without LAGs or other growth marks (e.g., Fig. S2).

Compared with the tibial sections, all fibular sections have relatively thick compact cortices and extremely small medullary cavities, which are surrounded by endosteal bone layers (Fig. 2). In the fibulae, the ratio of the medullary cavity to the compact cortex is large in the smallest specimen and relatively smaller in large individuals, and the largest specimen has the smallest ratio (Table 1). The cortices of the fibulae have fibrolamellar bone tissue as in the tibiae (Table 3), but parallel-fibered bone matrix under polarized light is present in the cortex adjacent to the tibiae in all samples (e.g., Figs. S1, S2). Most of the vascular canals are surrounded by lamellar bone, forming primary osteons. The vascular canals are mainly longitudinal. Transversely connected vascular canals, irregular canals, and trifurcate canals are less frequent than in the tibiae. The osteocyte lacunae are abundant as in those of the tibiae. Secondary osteons are common in the innermost region of the cortex in all but the smallest sampled individual. Due to minimal expansion of the medullary cavity, the number of visible LAGs in each fibula is equal to that in the corresponding tibia where comparisons are possible, but the innermost LAGs in all fibulae are better preserved (e.g., nearly completely surround the medullary cavity) than the corresponding tibial LAGs (Fig. 2), suggesting that the fibula is the

TABLE 2. Characteristic bone microstructure of the tibia in the three growth stages of *Jeholosaurus shangyuanensis*.

Characteristic	Stages		
	Early juvenile	Late juvenile	Subadult
Specimen number	IVPP V15719	IVPP V12529, IVPP V20380	IVPP V20379, IVPP V15939
Dominated bone tissue type	Fibrolamellar	Fibrolamellar	Fibrolamellar
Parallel-fibered bone in the outer cortex	No	No	Yes
Vascular canal shape	Mainly longitudinal and some radial orientated canals	Mainly longitudinal and some anastomosing, irregular, trifurcate canals	Mainly longitudinal and some anastomosing, irregular, trifurcate canals
Collagen fibers	Ordered, arranged near the periosteal margin in some areas	Ordered, arranged near the annuli (LAGs)	Ordered, arranged near the annuli (LAGs) and periosteal margin
Osteocyte lacunae	Globular	Flattened osteocyte lacunae appeared in the annuli (near LAGs)	Flattened osteocyte lacunae present in the annuli and outer region
Secondary reconstruction	None	Restricted to the corner contacting with the fibula	Restricted to the corner contacting with the fibula
Apparently reduced growth rate near the outermost region	No	No	Yes
Endosteal bone	Absent	Absent	Absent
LAG number	None	2 or 3	More than 4
LAG erosion	No	Yes	Yes

more reliable element compared with the tibia for skeletochronology in *Jeholosaurus*.

Histological Ontogenetic Stages

Some researchers refer to ontogenetic stages based on the attainment of adulthood at sexual maturity; however, definitive indicators of sexual maturity such as the presence of medullary bone (Lee and Werning, 2008) or gravidity (Sato et al., 2005) are relatively rarely identified in dinosaur fossils (Hone and Mallon, 2017) and are absent from our *Jeholosaurus* sample. We refer to ontogenetic stages based on relative somatic maturity and the attainment of adulthood when an individual has reached its largest body size and nearly stopped growing. This is often marked by the presence of an EFS (external fundamental system) in the outermost cortex (Horner et al., 2000).

The sample of *Jeholosaurus* can be divided into three stages according to bone histology and number of LAGs (Tables 1, 2). In this paper, the early juvenile is defined as an immature individual with uninterrupted growth. The late juvenile was still growing fast at death, but growth was interrupted by the formation of LAGs and/or annuli. In subadults, the individual apparently reduced its growth rate but had not yet reached somatic maturity. There are no somatically adult individuals in our sample, although some were likely sexually mature (see discussion of sexual maturity below).

Early Juvenile Stage—In the early juvenile stage (IVPP V15719; the tibial length is about 40% of that in the largest individual IVPP V15939), the bone mainly consists of woven-fibered matrix and is highly vascularized. Almost all the vascular canals are surrounded by lamellar bone, forming primary osteons, but there are also some simple vascular canals at the periphery. Abundant longitudinal vascular canals are arranged in a regular fashion forming radially oriented rows from the innermost cortex to the periphery in the cross-section of the tibia (Figs. 3A, 4; Fig. S1). Some oblique anastomosing canals are scattered in between the longitudinal canals (Figs. 3A, 4). The lateral surface articulating with the fibula is flattened and narrower than other regions. It is composed of highly organized parallel-fibered bone matrix under polarized light (Fig. S1E). The lateral corner is also composed of parallel-fibered bone matrix with densely organized fibers that parallel the lateral corner (Fig. S1D, E). A few primary osteons with vascular canals of larger diameter are also present in the lateral corner (Fig. S1A, E). There are no secondary osteons. Osteocyte lacunae are abundant and well organized around the vascular spaces. Abundant osteocyte lacunae are also present within the cortex bordering the medullary cavity and the subperiosteal surface. LAGs were not observed, but a thin bright birefringence appears near the periphery under polarized light (Fig. 3A; Fig. S1F), which suggests that this area grew slowly.

In the cross-section of the fibula, the thickness of the medial cortex (articulated with the tibia) is narrower than the lateral cortex and the medial surface for articulating with the tibia is flattened (Fig. 2F; Fig. S1). The medial cortex mainly consists of parallel-fibered bone matrix with seldom but large vascular canals, and dense fibers are visible under polarized light (Fig. S1), whereas the other parts are composed of woven-fibered bone. In the cortex, moderately dense vascular canals are predominately longitudinal, and vascular canals are more dense interiorly than exteriorly. Most canals are longitudinal primary osteons, and only a few simple canals are present at the periphery. There are no secondary osteons, LAGs, and annuli in the cortex. The endosteal bone is well preserved, with a thickness of 30 μm.

In general, the bone histology of IVPP V15719 suggests that it has a continuous rapid growth rate without apparent interruptions in this stage.

Late Juvenile Stage—IVPP V12529 and IVPP V20380 are considered late juveniles characterized by the presence of LAGs and moderately dense vascular canals in the outermost region (Fig. 2; Table 2). The smaller late juvenile (IVPP V12529) is about 44% of the body size (as measured from the anterior margin of the skull to the distal end of the ilium) of the largest specimen. In the tibial cross-section of the smaller individual, the cortex is organized in alternating zones and annuli (and LAGs). The zones consist of woven-fibered bone matrix and are highly vascularized. Almost all the vascular canals are primary osteons. The vascular canals are mainly longitudinal and anastomosing but also show some unorganized, irregularly oriented shapes (Figs. 3B, 4; Fig. S2). There are no secondary osteons except near the lateral corner connecting with the fibula. The annuli are very thin (about 20 μm), consisting of sparse longitudinal vascular canals and flattened osteocyte lacunae with the long axis aligned to the lamellar bone matrix. Two LAGs are clearly present in the cross-section, separating the cortex into three circumferential regions (Figs. 3B, 4). Although vascular canals are

TABLE 3. Characteristic bone microstructure of the fibula in the three growth stages of *Jeholosaurus shangyuanensis*.

	Stages		
Characteristic	Early juvenile	Late juvenile	Subadult
Specimen number	IVPP V15719	IVPP V12529, IVPP V20380	IVPP V20379, IVPP V15939
Dominated bone tissue type	Fibrolamellar	Fibrolamellar	Fibrolamellar
Parallel-fibered bone and lamellar bone in the outer cortex	No	No	Yes
Vascular canal shape	Mainly longitudinal, a few anastomosing canals	Mainly longitudinal, a few anastomosing, irregular and trifurcate canals	Mainly longitudinal, a few radial, irregular and trifurcate canals
Collagen fibers	Ordered, arranged near the periosteal margin in some areas	Ordered, arranged near the annuli (LAGs)	Ordered, arranged near the annuli (LAGs) and periosteal margin
Osteocyte lacunae	Globular	Flattened osteocyte lacunae appeared in the annuli (near LAGs)	Flattened osteocyte lacunae present in the annuli and outer region
Secondary reconstruction	None	Inner region	Inner region
Apparently reduced growth zone near the outermost region	No	No	Yes
Endosteal bone	Present	Present	Present
LAG number	None	2 or 3	More than 4
LAG erosion	No	Slightly	Slightly

abundant, the presence of LAGs demonstrates that rapid growth was periodically interrupted.

The bone tissue of the fibula shows moderately dense primary osteons that are predominantly longitudinal (Figs. 3, 4). A few secondary osteons are present in the innermost region (Fig. S2). Two LAGs are present in the cortex, as in the LAG number of the tibia. Endosteal bone tissue surrounding the medullary cavity is completely preserved and is thicker (about 60 μm) than in the sample of the early juvenile (IVPP V15719).

The tibial length of IVPP V20380 is 84% the tibial length of the largest individual IVPP V15939 and is much larger than the smaller late juvenile (IVPP V12529), with a tibial length 120% longer than the latter specimen. Compared with the smaller late juvenile (IVPP V12529), it contains more connected irregular and trifurcate canals (all are primary osteons) and the vascular canals are more dense, suggesting that it grew faster than IVPP V12529 in its first and second years (Montes et al., 2010) (Figs. 3C, 4; Fig. S3). Three LAGs are clearly present in both sampled sections. An innermost LAG is only partially preserved due to endosteal erosion. Two LAGs adjacent to each other are present at mid-cortex, and the outer LAG is far from the periphery, with a distance of 1.5 mm (Fig. 3). The presence of some open canals and no LAG at the periphery indicate that this individual was still growing rapidly when it died (Figs. 3C, 4).

The distance between adjacent LAGs is inconsistent in the large specimen (IVPP V20380) (Figs. 2C, 3C, 4, 5; Fig. S3). It grew much faster than the smaller late juvenile (IVPP V12529) and the smaller subadult individual (IVPP V20379) during the first two years based on the thickness of the cortex between LAGs. The distance from the centroid to LAG 2 in (IVPP V20380) is 100 μm larger than that in the late juvenile (IVPP V12529) and 60 μm larger than that in the subadult individual (IVPP V20379) (Fig. 5; Table S1). The cortex in IVPP V20380 is narrower between LAG 2 and LAG 3 but becomes wider again after LAG 3.

The cross-section of the fibula is elliptical in outline (Fig. 2H). The primary osteons are predominantly longitudinal. A few radially oriented canals are present in the outer region (most are primary osteons). Both the vascular canals and the osteocyte lacunae density are reduced toward the outer cortex. Several secondary osteons are concentrated within the innermost cortex. Three LAGs are present in the cortex, as in the tibia, but the innermost LAG is more completely preserved. The layer of

endosteal bone surrounding the medullary cavity is complete, with a thickness of about 60 μm.

Subadult Stage—The largest individual (IVPP V15939) and the third-largest individual (IVPP V20379) can be assigned to a subadult stage, which is defined by apparently reduced growth rates but without an EFS (Hone et al., 2016). They both have more than five LAGs and changes in tissue organization and/or adjacent LAG distance at the periphery (Table 2).

The tibial length of IVPP V20379 is 79% that of the largest individual (IVPP V15939). The cortex is moderately vascularized. Primary osteons are dominated throughout the cortex, and simple longitudinal vascular canals are shown in the outer cortex. Longitudinal and anastomosing canals are dominant, but there are also some irregular and trifurcate canals (Figs. 3D, E, 4; Fig. S4). There is no evidence of remodeling in the cortex except for the corner that articulates with the fibula. Five LAGs are present, but most of the innermost LAG is destroyed due to medullary expansion and breakage. The spacing between adjacent LAGs is gradually narrower toward the periphery, and the distance between the fourth and fifth LAGs is much less than between interior LAGs. Fibers or hydroxyapatite crystals appear under polarized light in this area and periphery, indicating that parallel-fibered bone tissue and the growth rate were dramatically decreased after the fourth LAG (Fig. 3E; Fig. S4).

The cross-section of the fibula extends anteroposteriorly and was compressed mediolaterally, with an elliptical outline. The bone mainly consists of woven-fibered bone matrix, and highly organized parallel-fibered bone is present in the medial cortex that contacts the fibula. The parallel-fibered bone transitioned to lamellar bone near the periphery (Fig. S4D). Most of the vascular canals are primary osteons, and a few longitudinal vascular canals are present in the outer region. The vascular canals are predominantly longitudinal, but several canals are radially oriented and cut through the LAGs in the middle and outermost cortex. The number of vascular canals decreased gradually toward the outermost region, and there are only a few vascular canals in the medial cortex that contacts the tibia. Secondary osteons are restricted to the innermost region of the cortex. Five LAGs are all clearly present in the cortex (Fig. 4; Fig. S4). The innermost LAG is very complete and was not affected by remodeling or enlargement of the medullary cavity.

In the largest specimen (IVPP V15939), the bone tissue is highly vascularized in the inner cortex and the primary osteons
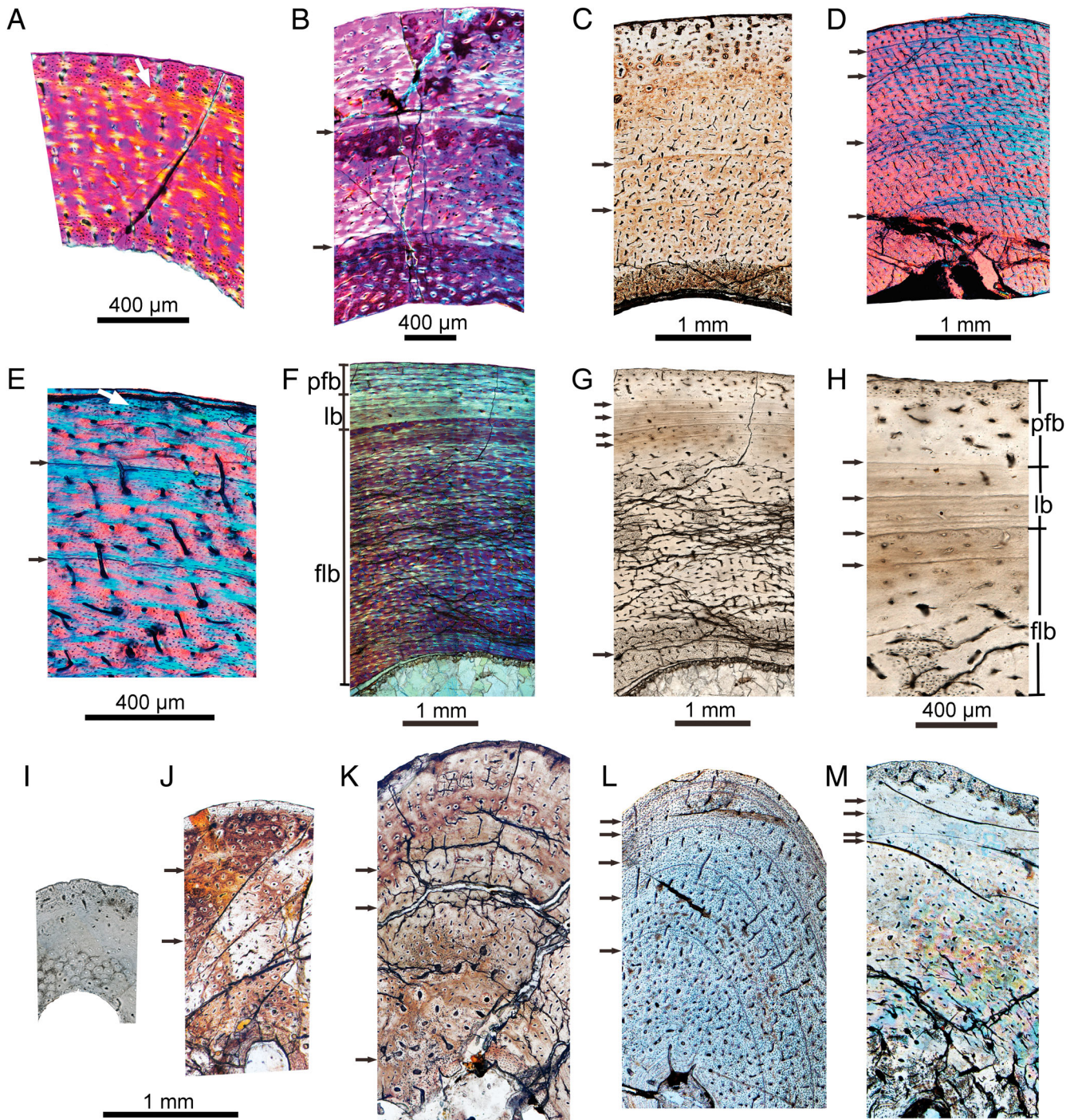
FIGURE 3. Bone microstructure in tibiae and fibulae of *Jeholosaurus shangyuanensis*. **A–H**, transverse sections of the tibiae: **A**, the smallest early juvenile individual IVPP V15719 under polarized light; **B**, smaller late juvenile specimen IVPP V12529 under polarized light; **C**, larger late juvenile specimen IVPP V20380 under normal light; **D**, smaller subadult specimen IVPP V20379 under polarized light; **E**, IVPP V20379 at higher magnification, showing the longitudinal primary osteons; **F**, large subadult individual IVPP V15939 under polarized light, showing fibrolamellar bone, parallel-fibered bone, and lamellar bone tissues; **G**, IVPP V15939 under normal light; **H**, IVPP V15939 at higher magnification, showing bone tissue types, dense LAGs, and vascular canals at the periphery. **I–M**, transverse sections of the fibulae under normal light: **I**, smallest early juvenile individual IVPP V15719; **J**, smaller late juvenile specimen IVPP V12529; **K**, larger late juvenile specimen IVPP V20380; **L**, smaller subadult specimen IVPP V20379; **M**, large subadult specimen IVPP V15939. Black arrows denote LAGs, and white arrows denote annuli (**A**, **E**, transversely oriented crystallites). **Abbreviations**: **fbl**, fibrolamellar bone; **lb**, lamellar bone; **pfb**, parallel-fibered bone.

form a reticular pattern. However, a series of closely spaced LAGs were present close to each other but not at the periphery of the cortex (about 400 μm to the periphery). This region is poorly vascularized, forming lamellar bone matrix with highly organized flattened osteocyte lacunae, of which the long axis extends along the orientation of LAGs (Figs. 3F–H, 4; Fig. S5).
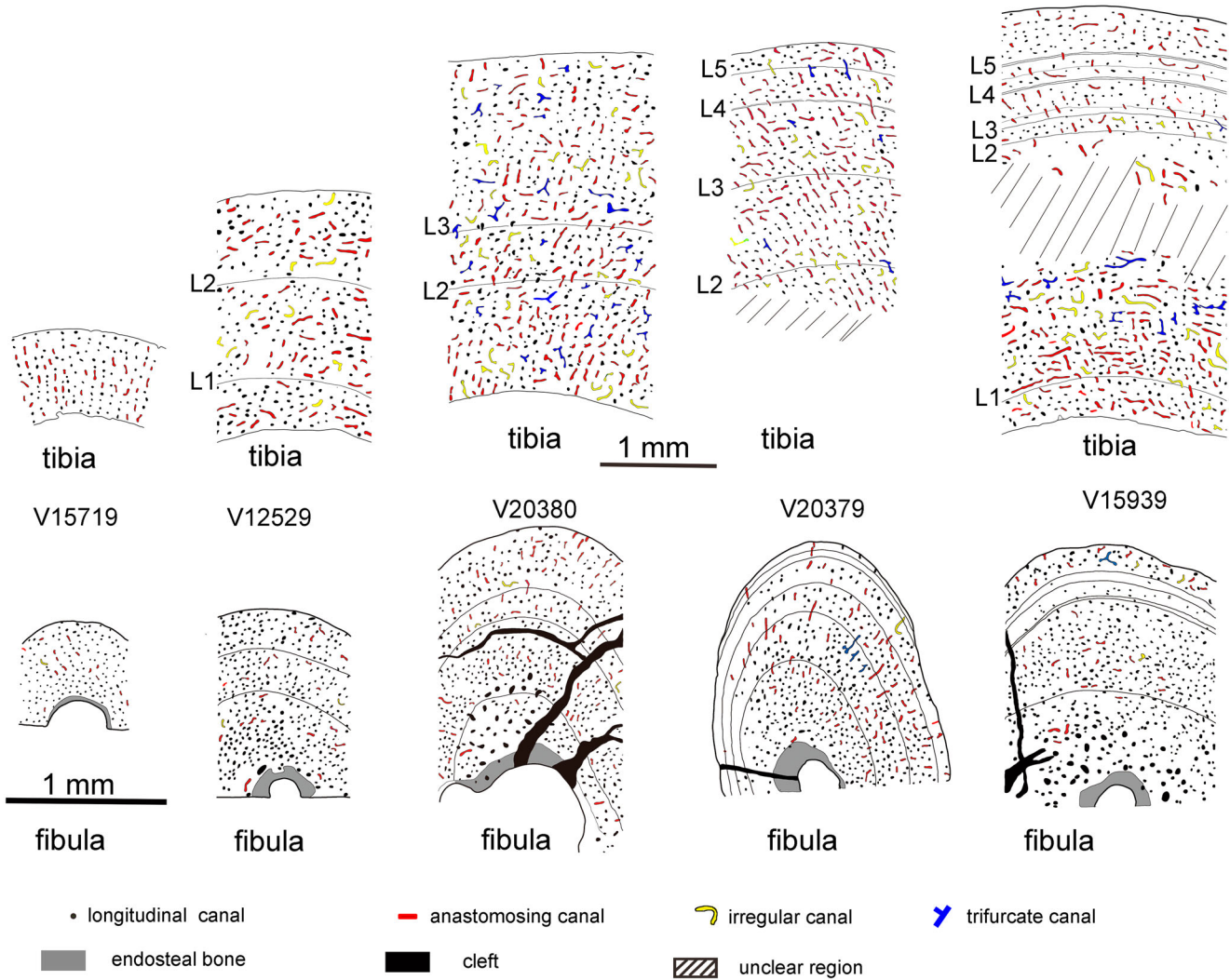
FIGURE 4. Line drawings of bone microstructure in tibiae and fibulae of *Jeholosaurus shangyuanensis*, showing LAGs and vascular density as well as arrangement/orientation of vascular canals. **Abbreviations**: **L1-5**, LAGs 1–5.

However, the bone matrix changing to parallel-fibered bone tissue with more vascular canals at the periosteal surface suggests that this individual was still growing at a moderate rate prior to death. The area with a series of LAGs as well as at least six weakly developed rest lines in the lamellar bone tissue. Particularly, double and triple LAGs are formed in some areas of the cortex but merge into a single LAG in other regions (Fig. 3G, H). Another prominent LAG is present in the innermost region and is completely preserved (Fig. 3G).

The cortex of the fibula is rounded and thickened with a small medullary cavity (Fig. 2I). A layer of endosteal bone tissue with a thickness of 80 µm was present (Fig. S5). Vascular canals are longitudinal and abundant throughout the cortex, and most vascular canals are primary osteons. A few longitudinal vascular canals are present in the outer cortex. Secondary osteons are restricted to the innermost region. Dense Sharpey's fibers are present in the region that contacts the fibula (Fig. S5H). One LAG was detected near the inner cortex. As in the tibia, a series of LAGs are shown near the outermost region and four LAGs are prominent (Fig. 4; Fig. S5), but the inner two LAGs are close to each other and merged into one in some places (Fig. 2J). The area with a series of LAGs has a thickness of about 240 µm. The

highly organized collagen fibers with rare vascular canals and highly organized flattened osteocytes suggest the deposition of lamellar bone tissue in this area. However, the bone matrix changed to parallel-fibered bone and vascular canals apparently increased at the periphery, with a thickness of about 120 µm.

In general, the dominantly fibrolamellar organization of *Jeholosaurus* indicates that it had a rapid growth rate that was interrupted in forming LAGs, as in other small ornithopods such as *Orodromeus* (Horner et al., 2009). The distances between adjacent LAGs are gradually reduced in the juvenile individual IVPP V12529 and the subadult IVPP V20379 but are variable in the large juvenile IVPP V20380 and the large subadult IVPP V15939. There are no secondary osteons in any tibial sections, but they are present within the innermost growth zones of the fibula. Endosteal bone is well preserved in all fibulae but is absent in all tibial sections.

DISCUSSION

Age Estimation

Age estimation was based on counting the number of LAGs in the tibia and fibula. We hypothesize that the smallest specimen
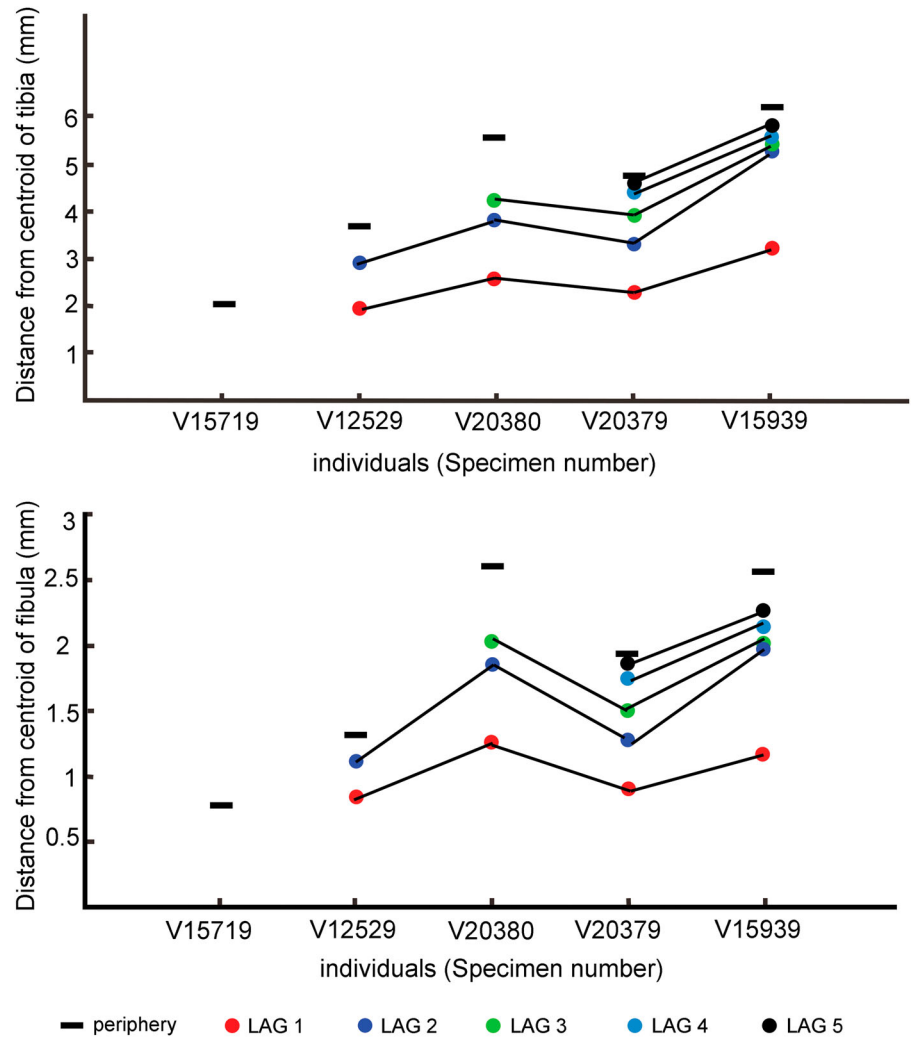
FIGURE 5. Comparison of the cortical thickness of tibiae and fibulae for each year (determined by the number of LAGs) in every specimen of *Jeholosaurus*.

(IVPP V15719) comes from an individual less than one year old because there are no LAGs preserved in either the tibial or the fibular section (Figs. 2, 3A; Table 1), and because the fibular medullary cavity is less than 1 mm in diameter, indicating minimal loss of primary tissue due to medullary expansion. Although the tibia and fibula of the holotype specimen (IVPP V12529) were crushed during preservation and portions of the tibial cortex are missing from the section, two LAGs can be recognized in both bones. The innermost LAG in the fibula is completely preserved and only partially covered by secondary osteons, which indicates that it died after two years of age given the relative size of the fibular cross-section lacking growth marks of IVPP V15719. The late juvenile individual (IVPP V20380) has a tibial length 1.2 times that of the smaller late juvenile (IVPP V12529), but it only has three LAGs, and much of the innermost LAG has been eroded by the expansion of the medullary cavity. Comparison with the smaller specimen IVPP V12529 suggests that the innermost LAG represents the first LAG. Therefore, IVPP V20380 likely died at three years old. Five LAGs are present in the subadult individual IVPP 20379 and the largest individual IVPP V15939, but their distribution is quite different. In the smaller subadult individual IVPP V20379, the outer four LAGs are distinctly separated from each other and almost completely encircle the medullary cavity, except in the area of

fibular contact. The innermost tibial LAG of the smaller subadult individual IVPP V20379 has been partially destroyed due to preservation but is well preserved in the fibula (Fig. S4). In the largest individual (IVPP V15939), there is a LAG at the innermost region, and a region closer to the periphery of the cortex with four clear LAGs as well as numerous closely packed rest lines that are far from the innermost LAG. The feature we interpret as the innermost LAG of IVPP V15939 (Fig. 4) likely represents the first annual growth mark and corresponds to the approximate location of the first LAG when compared with smaller specimens. Therefore, the age of IVPP V20379 and the largest individual IVPP V15939 is probably five years, although they have different body sizes and growth patterns.

In fibulae, the number of LAGs is consistent with that of corresponding tibiae for all sections except the largest individual (IVPP V15939). The fibula of IVPP V15939 contains four LAGs: an innermost LAG and three other closely packed LAGs as well as several rest lines near the periphery (Fig. S5), similar to the pattern in the tibia of the same specimen. The three tightly packed LAGs sometimes appear to separate into four, likely reflecting slow growth, with bone being deposited in the areas of the split and nondeposition in the regions without a split LAG (Fig. S5).

Overall, the fibular LAGs of *Jeholosaurus* experienced less erasure due to medullary expansion, providing a better skeletochronological record than those of the tibiae. However, the LAGs could be missed or undetected if they are closely adjacent to each other. Therefore, both the tibial and fibular sections are necessary in order to obtain an accurate age estimation of this ornithopod.

Sexual Maturity

The attainment of sexual maturity is usually accompanied by apparently reduced growth rates in extant reptiles (Brody, 1964; Andrews, 1982; Reiss, 1989; Shine and Charnov, 1992). Research evaluating the earliest ontogenetic appearance of medullary bone in concert with growth curve estimation based on skeletochronology suggests that dinosaurs reached sexual maturity long before somatic maturity and that growth rates decrease following its attainment (Lee and Werning, 2008). This could result in changes in bone tissue organization and/or decreasing distance between adjacent LAGs (Klein and Sander, 2007). Because these features are not always necessarily present together, either feature shown may suggest sexual maturity, but other factors potentially responsible for the slowed deposition of bone, such as environmental conditions, cannot be excluded when interpreting dinosaur life histories from small sample sizes. Reduced growth rates are apparent in the largest individual (IVPP V15939), the smaller subadult individual (IVPP V20379), and the large late juvenile (IVPP V20380) at different ages. Both smaller distances between LAGs and a change from dominantly fibrolamellar bone to parallel-fibered bone are present in the largest individual (IVPP V15939), but only a decrease in distance between LAGs is present in the outer cortex in the other two specimens.

In the largest specimen (IVPP V15939; tibial length of 161 mm), the width between adjacent LAGs is very narrow following the second LAG, and the change in tissue organization from fibrolamellar bone to lamellar bone and parallel-fibered bone occurs after the third LAG and persists until the outermost region of the cortex. Although vascular canals are slightly increased at the periphery, the density of vascular canals present in the first two growth zones never reaches the density present in the first two growth zones. Thus, the bone tissue changes suggest the attainment of sexual maturity after two years old.

In the smaller subadult individual (IVPP V20379; tibial length of 127 mm), the distance between adjacent LAGs is gradually reduced for earlier growth zones, but there is an obvious decrease in depositional rate after the fourth LAG. Sexual maturity probably corresponds to the decrease in depositional rate in the fourth to fifth years.

In the large juvenile individual (IVPP V20380; tibial length of 135 mm), a much narrower zone is present between LAG 2 and LAG 3. However, the width between LAG 3 and the periphery is much wider than the former, suggesting that it grew much faster at three years old than at two years old. The irregular distribution of LAGs does not support the attainment of sexual maturity but indicates that the individual was still growing at comparable rates to its juvenile ontogeny before death.

Surprisingly, the attainment of sexual maturity is either not uniform in *Jeholosaurus* or is not recorded uniformly in its bone histology. This phenomenon is also seen in some extant tetrapods, where intraspecific variability in the attainment of sexual maturity may be caused by sexual differences and/or variable rates of attainment of a threshold body size. Skeletochronological studies of salamanders indicate that the timing of sexual maturation is different in male and female individuals, and the latter is usually one or two years later than the former (Castanet et al., 1996; Misawa and Matsui, 2000). In some extant lizards, sexual maturity appears to be determined by a minimum size

rather than age as a result of highly variable growth rates (Bauwens and Verheyen, 1987; Galán, 1996). However, this phenomenon appears to be restricted to short-lived organisms (e.g., lizards) that reach sexual maturity at one or two years old and is poorly known in long-lived species. In crocodiles, females attain sexual maturity after their body length reaches 262 to 287 cm, whereas males reach sexual maturity at body lengths between 270 and 295 cm (Kofron, 1990), but whether they attained sexual maturity at the same age is poorly known.

In conclusion, the attainment of sexual maturity in *Jeholosaurus* likely occurs between two and four years of age, which is similar to that of other ornithopod dinosaurs such as *Orodromeus* (Horner et al., 2009), a small 'hypsilophodontid' from the Antarctic circle (Woodward et al., 2011), and the large hadrosaur *Maiasaura* (Woodward et al., 2015). *Orodromeus* is a small Late Cretaceous ornithopod that is closely related to the Early Cretaceous *Jeholosaurus* (Han et al., 2012). It has a relatively small body size, roughly comparable to *Jeholosaurus*, but the largest known individual of *Jeholosaurus* (IVPP V15939; tibial length equals 161 mm) is slightly smaller than the adult size of *Orodromeus* (MOR 973-T-2; tibial length equals 195 mm; Horner et al., 2009). However, *Orodromeus* has LAGs near the periphery only in subadult and adult individuals, and the number of LAGs (only three in the adult individual) is less than that of *Jeholosaurus*. This suggests that sexual maturity of *Orodromeus* was likely attained earlier than in *Jeholosaurus*. Surprisingly, the likely attainment of sexual maturity of the hadrosaur *Maiasaura* was three years old on the basis of a large-sample statistical assessment (Woodward et al., 2015), whereas it is apparently much later in many iguanodontians, such as *Dysalotosaurus* (10 LAGs; Hübner, 2012) and *Tenontosaurus* (7 or 8 LAGs; Lee and Werning, 2008), as well as in the ceratopsian *Psittacosaurus* (9 LAGs; Erickson et al., 2009). It seems that the timing at which sexual maturity attained is highly variable among ornithopod dinosaurs, with early sexual maturation present in *Jeholosaurus* and other small ornithopods as well as some large-bodied hadrosaurs.

Growth Variation

The smaller late juvenile (IVPP V12529) and the smaller subadult individual IVPP V20379 show fibrolamellar bone tissue that was interrupted forming LAGs and annuli, and growth rates gradually reduced. In the largest individual IVPP V15939, the thickness of the cortex at two years old has already reached those of the smaller subadult individuals IVPP V20379 at the fifth year and IVPP V20380 at four years old (Fig. 5), but closely packed LAGs including double or triple LAGs and lamellar bone tissue appeared after the second year. The rapid growth rate until sexual maturity and apparently slow down after that is quite different from all other specimens but is similar to extant birds and mammals (Chinsamy-Turan, 2005), and the only distinction is that the dense LAGs are not preserved at the periphery. Therefore, the growth rates of *Jeholosaurus* vary according to year across individuals. This may be caused by variable environmental conditions (Hübner et al., 2012), individual variation, or sexual dimorphism (Sander, 2000).

Environmental conditions that strongly affect body size are known to have a histological signature in the bones of some extant lizards, especially in juvenile individuals (Petermann et al., 2017). Mammals are also known to experience slowed growth rates and to produce LAGs in resource-limited habitats (Köhler and Moyà-Solà, 2009). In the largest individual (IVPP V15939), double and triple LAGs are present near the periphery of the cortex, and these features may indicate that the individual experienced harsh environmental conditions, as demonstrated in species across a wide taxonomic range including amphibians, reptiles, and mammals (Castanet, 1994; Esteban et al., 1996; Botha

and Chinsamy, 2004; Köhler and Moyà-Solà, 2009; Sanchez et al., 2010). Therefore, the closely packed LAGs may indicate a harsh environment.

Intraspecific variation in development unrelated to sexual maturity or the environment is also a factor that affects growth rates in extant animals (e.g., tortoises, Lagarde et al., 2001) and may affect the bone tissue type and the distance between LAGs. However, there is still no evidence that shows that this type of individual variation could produce closely spaced LAGs.

Sexual dimorphism can take the form of differences in body size, shape, or extreme morphologies present in one sex (Chapman et al., 1997), but statistical analyses suggest that sexual dimorphism in dinosaurs is difficult to demonstrate (Hone and Mallon, 2017; Mallon, 2017). The only definitive method for identifying individual sex in Mesozoic dinosaurs is the identification of female-specific tissues such as medullary bone (Schweitzer et al., 2005; Lee and Werning, 2008) (although recent studies questioned whether these tissues were correctly identified; Chinsamy and Tumarkin-Deratzian, 2009; Prondvai and Stein, 2014; Chinsamy et al., 2016; Prondvai, 2017) or the identification of gravid individuals (Sato et al., 2005; Bailleul et al., 2019). Therefore, proposed instances of sexually dimorphic structures or growth patterns cannot be associated with male or female sex in most cases. In extant reptiles, sexual size dimorphism can be demonstrated by variable growth trajectories according to sex. In some cases, male and female individuals have similar growth rates until sexual maturity, at which point one sex grows faster than the other (Andrews, 1982). Alternatively, one sex sometimes grows faster than the other throughout life and a size disparity between the sexes is already present at sexual maturity (Andrews, 1982). The unusual growth pattern of the largest individual IVPP V15939 is more in accordance with the second pattern.

Aside from sex-specific tissues such as medullary bone, sex differences in tissue organization or growth rate have only rarely been commented upon in the non-avian dinosaurian literature. Sander (2000) tentatively interpreted sex differences in *Barosaurus* based on an apparently dimorphic histological pattern, but the small sample size of one of the apparent morphs could not preclude the influence of other factors, such as environmental conditions, individual variation, or taxonomic variation. A large histological data set of *Plateosaurus* showed a high variation in growth rates, but sexual dimorphism was not detected in this taxon (Klein and Sander, 2007). Therefore, testing whether the observed variability in the growth trajectory of *Jeholosaurus* is a sexually dimorphic pattern will require a much larger sample size.

Implications for Environment and Development

The largest individual (IVPP V15939) possesses a series of LAGs (including double LAGs) closely packed together near the peripheral region (about 400 µm to the periphery), which suggests that it experienced a long slow growth period (Fig. 3H). However, no LAGs and a few vascular canals are present in the outermost region, indicating that the bone was still growing before it died (faster than the region with closely spaced LAGs). Closely packed LAGs followed by a few vascular canals and no LAGs seem to be unusual in dinosaur bone tissue. Here, we propose three hypotheses to explain this phenomenon.

The unusual feature may be caused by changing environmental conditions. The closely packed LAGs may indicate a harsh environment, and the relatively higher growth rates at the periphery suggest a return to more tolerable conditions, such as the relative abundance of food or warm weather.

Other explanations of this unusual bone tissue type include factors intrinsic to the individuals themselves, such as pathology or behavior. The histological consequences of externally manifesting pathologies have been studied in a fractured fibula of

Psittacosaurus in which it shows radially oriented spokes of woven bone (Hedrick et al., 2016). However, no external evidence of pathology can be identified in the largest individual (IVPP V15939). The bone tissue is also unlike the pathological tissues described in previous papers (Chinsamy and Tumarkin-Deratzian, 2009; Griffin, 2018). A third explanation is that the largest individual IVPP V15939 may have to take care of young (parental care or posthatching cooperation) following the attainment of sexual maturity, which may consume larger amounts of energy (Gittleman and Thompson, 1988). This may reduce growth rates and narrow the distance between adjacent LAGs (Zhao et al., 2014).

Parental care in dinosaurs has been supported by previous studies (Varricchio, 2011). Parental care was suggested in troodontid and oviraptorid dinosaurs based on a statistical analysis of the clutch volume of brooding adults, and this may represent ancestral condition for birds (Varricchio et al., 2008). Additionally, parental care was suggested to have been present in the hadrosaur *Maiasaura* from the Two Medicine Formation near Choteau, Montana, on the basis of a nest of juvenile individuals. The discovery of 15 1-m-long hadrosaurian skeletons together suggests that they may have lived together and were cared for by their parents (Horner and Makela, 1979; Horner et al., 2001). Moreover, *Psittacosaurus* was supposed to exhibit parental care based on the discovery of a large *Psittacosaurus* and 34 young conspecifics found together from the Lower Cretaceous of Liaoning Province, China (Meng et al., 2004). This provides strong evidence that at least some non-avian dinosaurs cared for their young. However, recent research indicates that the large *Psittacosaurus* individual may not have reached sexual maturity (Zhao et al., 2014) but may be an example of posthatching cooperation (Hedrick et al., 2014). Bone histological information of this large *Psittacosaurus* could show whether it has reached sexual maturity and may help to clarify whether it is parental care or posthatching cooperation.

Whether parental care or posthatching cooperation could affect bone tissue is poorly known across tetrapods. However, Zhao et al. (2014) provided clear evidence of different age clusters in *Psittacosaurus*, finding that the older individual possessed a much narrower cortex and fewer vascular canals at three years of life than in the first two years. Therefore, it is possible that this behavior could affect the bone tissue structure in the largest individual (IVPP V15939).

CONCLUSIONS

The bone histology of *Jeholosaurus* consists of fibrolamellar bone tissue in early ontogenetic stages that indicates rapid growth rates with interruptions (indicated by LAGs), as in other small ornithopods. According to bone tissue type and LAG intervals, two different growth patterns occur in the sampled *Jeholosaurus* material that may suggest sexual dimorphism or variable environmental conditions. One type grows fast at an early stage, and growth is gradually reduced in later ontogenies, such as in the smaller subadult individual IVPP V20379. This pattern may be the result of variable environmental conditions and/or individual variation, resulting in growth differences every year (e.g., IVPP V20380). The other type shows fast growth rates during the first two years but strongly reduced growth in later ontogeny, marked by the formation of lamellar bone tissues and the deposition of closely spaced LAGs (e.g., the largest individual IVPP V15939). Based on bone tissue changes and decreasing LAG intervals, we hypothesize that sexual maturity occurred at two years old in the largest individual IVPP V15939 and four years old in the smaller subadult individual IVPP V20379. Therefore, the age of sexual maturity would probably be between two and four years old, as in some other small ornithopods and the hadrosaur *Maiasaura* (Woodward et al.,

2015), but earlier than that of *Dysalotosaurus* and *Psittacosaurus* (Erickson et al., 2009; Hübner, 2012). The relatively early sexual maturity of *Jeholosaurus* may indicate a successful survival strategy. In the largest individual IVPP V15939, vascular canals and no LAGs present at the periphery suggest that it still grew after a long slow growth period (indicating by several closely spaced LAGs). This unusual feature may be an indicator of an environmental condition or social behavior in these small ornithischians. However, all these issues need to be clarified based on a large data set of bone tissue in the future.

LITERATURE CITED

Abràmoff, M. D., P. J. Magalhães, and S. J. Ram. 2004. Image processing with ImageJ. Biophotonics International 11:36–42.

Andrews, R. M. 1982. Patterns of growth in reptiles; pp. 273–320 in C. Gans and F. H. Pough (eds.), Biology of the Reptilia. Vol. 13. Academic Press, London, U.K.

Bailleul, A. M., J. O'Connor, S. Zhang, Z. Li, Q. Wang, M. C. Lamanna, X. Zhu, and Z. Zhou. 2019. An Early Cretaceous enantiornithine (Aves) preserving an unlaid egg and probable medullary bone. Nature Communications 10:1275.

Barrett, P. M., and F.-L. Han. 2009. Cranial anatomy of *Jeholosaurus shangyuanensis* (Dinosauria: Ornithischia) from the Early Cretaceous of China. Zootaxa 2072:31–55.

Bauwens, D., and R. F. Verheyen. 1987. Variation of reproductive traits in a population of the lizard *Lacerta vivipara*. Ecography 10:120–127.

Botha, J., and A. Chinsamy. 2004. Growth and life habits of the Triassic cynodont *Trirachodon*, inferred from bone histology. Acta Palaeontologica Polonica 49:619–627.

Brody, S. 1964. Bioenergetics and Growth: With Special Reference to the Efficiency Complex in Domestic Animals. Hafner Publishing, New York, 1023 pp.

Butler, R. J., P. Upchurch, and D. B. Norman. 2008. The phylogeny of the ornithischian dinosaurs. Journal of Systematic Palaeontology 6:1–40.

Bybee, P. J., A. H. Lee, and E. T. Lamm. 2006. Sizing the Jurassic dinosaur *Allosaurus*: assessing growth strategy and evolution of ontogenetic scaling of limbs. Journal of Morphology 267:347–359.

Castanet, J. 1994. Age estimation and longevity in reptiles. Gerontology 40:174–192.

Castanet, J., H. Francillon-Vieillot, and R. C. Bruce. 1996. Age estimation in desmognathine salamanders assessed by skeletochronology. Herpetologica 52:160–171.

Castanet, J., H. Francillon-Vieillot, F. J. Meunier, and A. de Ricqlès. 1993. Bone and individual aging; pp. 245–283 in B. Hall (ed.), Bone, Volume 7, Bone Growth. CRC Press, Boca Raton, Florida.

Cerda, I. A., and A. Chinsamy. 2012. Biological implications of the bone microstructure of the Late Cretaceous ornithopod dinosaur *Gasparinisaura cincosaltensis*. Journal of Vertebrate Paleontology 32:355–368.

Chapman, R. E., D. B. Weishampel, G. Hunt, and Rasskin-Gutman. 1997. Sexual dimorphism in dinosaurs; pp. 83–93 in D. L. Wolberg, E. Stump, and G. Rosenberg (eds.), Dinofest International. Philadelphia Academy of Natural Sciences, Philadelphia, Pennsylvania.

Chinsamy, A. 1995. Ontogenetic changes in the bone histology of the Late Jurassic ornithopod *Dryosaurus lettowvorbecki*. Journal of Vertebrate Paleontology 15:96–104.

Chinsamy, A., and A. Tumarkin-Deratzian. 2009. Pathologic bone tissues in a turkey vulture and a nonavian dinosaur: implications for interpreting endosteal bone and radial fibrolamellar bone in fossil dinosaurs. The Anatomical Record 292:1478–1484.

Chinsamy, A., I. Cerda, and J. Powell. 2016. Vascularised endosteal bone tissue in armoured sauropod dinosaurs. Scientific Reports 6:24858.

Chinsamy-Turan, A. 2005. The Microstructure of Dinosaur Bone. Johns Hopkins University Press, Baltimore, Maryland, 195 pp.

Donath, K., and M. Rohrer. 2003. Bone sectioning using the Exakt system; pp. 243–252 in Y. H. An and K. L. Martin (eds.), Handbook of Histology Methods for Bone and Cartilage. Springer, Dordrecht, The Netherlands.

Erickson, G. M. 2005. Assessing dinosaur growth patterns: a microscopic revolution. Trends in Ecology and Evolution 20:677–684.

Erickson, G. M., and T. A. Tumanova. 2000. Growth curve of *Psittacosaurus mongoliensis* Osborn (Ceratopsia: Psittacosauridae) inferred from long bone histology. Zoological Journal of the Linnean Society 130:551–566.

Erickson, G. M., K. C. Rogers, and S. A. Yerby. 2001. Dinosaurian growth patterns and rapid avian growth rates. Nature 412:429–433.

Erickson, G. M., K. Curry Rogers, D. J. Varricchio, M. A. Norell, and X. Xu. 2007. Growth patterns in brooding dinosaurs reveals the timing of sexual maturity in non-avian dinosaurs and genesis of the avian condition. Biology Letters 3:558–561.

Erickson, G. M., P. J. Makovicky, B. D. Inouye, C.-F. Zhou, and K.-Q. Gao. 2009. A life table for *Psittacosaurus lujiatunensis*: initial insights into ornithischian dinosaur population biology. The Anatomical Record 292:1514–1521.

Erickson, G. M., P. J. Makovicky, P. J. Currie, M. A. Norell, S. A. Yerby, and C. A. Brochu. 2004. Gigantism and comparative life-history parameters of tyrannosaurid dinosaurs. Nature 430:772–775.

Esteban, M., M. García-París, and J. Castanet. 1996. Use of bone histology in estimating the age of frogs (*Rana perezi*) from a warm temperate climate area. Canadian Journal of Zoology 74:1914–1921.

Francillon-Vieillot, H., V. de Buffrénil, J. Castanet, J. Géraudie, F. J. Meunier, J. Y. Dire, L. Zylberberg, and A. de Ricqlès. 1990. Microstructure and mineralization of vertebrate skeletal tissues; pp. 471–530 in J. G. Carter (ed.), Skeletal Biomineralization: Patterns, Processes and Evolutionary Trends. Van Nostrand Reinhold, New York.

Galán, P. 1996. Sexual maturity in a population of the lacertid lizard *Podarcis bocagei*. Herpetological Journal 6:87–93.

Gittleman, J. L., and S. D. Thompson. 1988. Energy allocation in mammalian reproduction. Integrative and Comparative Biology 28:863–875.

Gotfredsen, K., E. Budtz-Jørgensen, and L. N. Jensen. 1989. A method for preparing and staining histological sections containing titanium implants for light microscopy. Stain Technology 64:121–127.

Grady, J. M., B. J. Enquist, E. Dettweiler-Robinson, N. A. Wright, and F. A. Smith. 2014. Evidence for mesothermy in dinosaurs. Science 344:1268–1272.

Griffin, C. T. 2018. Pathological bone tissue in a Late Triassic neotheropod fibula, with implications for the interpretation of medullary bone. New Jersey State Museum Investigations 6:2–10

Hübner, T. R. 2012. Bone histology in *Dysalotosaurus lettowvorbecki* (Ornithischia: Iguanodontia)—variation, growth, and implications. PLoS ONE 7:e29958.

Han, F.-L., P. M. Barrett, R. J. Butler, and X. Xu. 2012. Postcranial anatomy of *Jeholosaurus shangyuanensis* (Dinosauria, Ornithischia) from the Lower Cretaceous Yixian Formation of China. Journal of Vertebrate Paleontology 32:1370–1395.

He, H. Y., X. L. Wang, Z. H. Zhou, F. Jin, F. Wang, L. K. Yang, X. Ding, A. Boven, and R. X. Zhu. 2006. Ar-40/Ar-39 dating of Lujiatun bed (Jehol group) in Liaoning, northeastern China. Geophysical Research Letters 33:1–4.

Hedrick, B. P., C. Gao, G. I. Omar, F. Zhang, C. Shen, and P. Dodson. 2014. The osteology and taphonomy of a *Psittacosaurus* bonebed assemblage of the Yixian Formation (Lower Cretaceous), Liaoning, China. Cretaceous Research 51:321–340.

Hedrick, B. P., C. Gao, A. R. Tumarkin-Deratzian, C. Shen, J. L. Holloway, F. Zhang, K. D. Hankenson, S. Liu, J. Anné, and P. Dodson. 2016. An injured *Psittacosaurus* (Dinosauria: Ceratopsia) from the Yixian

Formation (Liaoning, China): implications for *Psittacosaurus* biology. The Anatomical Record 299:897–906.

Horner, J. R., K. Padian, and A. de Ricqlès. 2001. Comparative osteohistology of some embryonic and perinatal archosaurs: developmental and behavioral implications for dinosaurs. Paleobiology 27:39–58.

Hone, D. W. E., and J. C. Mallon. 2017. Protracted growth impedes the detection of sexual dimorphism in non-avian dinosaurs. Palaeontology 60:535–545.

Hone, D. W. E., A. A. Farke, and M. J. Wedel. 2016. Ontogeny and the fossil record: what, if anything, is an adult dinosaur? Biology Letters 12:20150947.

Horner, J. R., and R. Makela. 1979. Nest of juveniles provides evidence of family structure among dinosaurs. Nature 282:296–298.

Horner, J. R., and K. Padian. 2004. Age and growth dynamics of *Tyrannosaurus rex*. Proceedings of the Royal Society of London, Series B: Biological Sciences 271:1875–1880.

Horner, J. R., A. de Ricqles, and K. Padian. 1999. Variation in dinosaur skeletochronology indicators: implications for age assessment and physiology. Paleobiology 25:295–304.

Horner, J. R., A. de Ricqles, and K. Padian. 2000. Long bone histology of the hadrosaurid dinosaur *Maiasaura peeblesorum*: growth dynamics and physiology based on an ontogenetic series of skeletal elements. Journal of Vertebrate Paleontology 20:115–129.

Horner, J. R., A. de Ricqlès, K. Padian, and R. D. Scheetz. 2009. Comparative long bone histology and growth of the "hypsilophodontid" dinosaurs *Orodromeus makelai*, *Dryosaurus altus*, and *Tenontosaurus tilletti* (Ornithischia: Euornithopoda). Journal of Vertebrate Paleontology 29:734–747.

Köhler, M., and S. Moyà-Solà. 2009. Physiological and life history strategies of a fossil large mammal in a resource-limited environment. Proceedings of the National Academy of Sciences of the United States of America 106:20354–20358.

Klein, N., and P. M. Sander. 2007. Bone histology and growth of the prosauropod dinosaur *Plateosaurus engelhardti* von Meyer, 1837 from the Norian bonebeds of Trossingen (Germany) and Frick (Switzerland). Special Papers in Palaeontology 77:169–206.

Klein, N., and P. M. Sander. 2008. Ontogenetic stages in the long bone histology of sauropod dinosaurs. Paleobiology 34:247–263.

Kofron, C. P. 1990. The reproductive cycle of the Nile crocodile (*Crocodylus niloticus*). Journal of Zoology 221:477–488.

Lagarde, F., X. Bonnet, B. T. Henen, J. Corbin, K. A. Nagy, and G. Naulleau. 2001. Sexual size dimorphism in steppe tortoises (*Testudo horsfieldi*): growth, maturity, and individual variation. Canadian Journal of Zoology 79:1433–1441.

Lee, A. H., and P. M. O'Connor. 2013. Bone histology confirms determinate growth and small body size in the noasaurid theropod *Masiakasaurus knopfleri*. Journal of Vertebrate Paleontology 33:865–876.

Lee, A. H., and S. Werning. 2008. Sexual maturity in growing dinosaurs does not fit reptilian growth models. Proceedings of the National Academy of Sciences of the United States of America 105:582–587.

Lee, A. H., A. K. Huttenlocker, K. Padian, and H. N. Woodward. 2013. Analysis of growth rates; pp. 217–251 in K. Padian and E. T. Lamm (eds.), Bone Histology of Fossil Tetrapods: Advancing Methods, Analysis, and Interpretation. University of California Press, Berkeley, California.

Mallon, J. C. 2017. Recognizing sexual dimorphism in the fossil record: lessons from nonavian dinosaurs. Paleobiology 43:495–507.

Meng, Q., J. Liu, D. J. Varricchio, T. Huang, and C. Gao. 2004. Palaeontology: parental care in an ornithischian dinosaur. Nature 431:145–146.

Misawa, Y., and M. Matsui. 2000. Age determination by skeletochronology of the Japanese salamander *Hynobius kimurae* (Amphibia, Urodela). Zoological Science 17:253–257.

Montes, L., J. Castanet, and J. Cubo. 2010. Relationship between bone growth rate and bone tissue organization in amniotes: first test of Amprino's rule in a phylogenetic context. Animal Biology 60:25–41.

Norman, D. B., H.-D. Sues, L. M. Witmer, and R. A. Coria. 2004. Basal Ornithopoda; pp. 393–412 in D. B. Weishampel, P. Dodson, and H. Osmólska (eds.), The Dinosauria, second edition. University of California Press, Berkeley, California.

Padian, K., A. J. de Ricqles, and J. R. Horner. 2001. Dinosaurian growth rates and bird origins. Nature 412:405–408.

Petermann, H., N. M. Koch, and J. A. Gauthier. 2017. Osteohistology and sequence of suture fusion reveal complex environmentally influenced growth in the teiid lizard *Aspidoscelis tigris*—implications for fossil squamates. Palaeogeography, Palaeoclimatology, Palaeoecology 475:12–22.

Prondvai, E. 2017. Medullary bone in fossils: function, evolution and significance in growth curve reconstructions of extinct vertebrates. Journal of Evolutionary Biology 30:440–460.

Prondvai, E., and K. H. W. Stein. 2014. Medullary bone-like tissue in the mandibular symphyses of a pterosaur suggests non-reproductive significance. Scientific Reports 4:6253.

Reiss, M. J. 1989. The Allometry of Growth and Reproduction. Cambridge University Press, Cambridge, U.K., 82 pp.

Reizner, J. A. 2010. An ontogenetic series and population histology of the ceratopsid dinosaur *Einiosaurus procurvicornis*. M.Sc. thesis, Montana State University, Bozeman, Montana, 97 pp.

Sanchez, S., J. S. Steyer, R. R. Schoch, and A. de Ricqlès. 2010. Palaeoecological and palaeoenvironmental influences revealed by long-bone palaeohistology: the example of the Permian branchiosaurid *Apateon*. Geological Society, London, Special Publications 339:139–149.

Sander, P. M. 2000. Longbone histology of the Tendaguru sauropods: implications for growth and biology. Paleobiology 26:466–488.

Sander, P. M., O. Mateus, T. Laven, and N. Knotschke. 2006. Bone histology indicates insular dwarfism in a new Late Jurassic sauropod dinosaur. Nature 441:739–741.

Sato, T., Y. N. Cheng, X. C. Wu, D. K. Zelenitsky, and Y. F. Hsiao. 2005. A pair of shelled eggs inside a female dinosaur. Science 308:375.

Schweitzer, M. H., J. L. Wittmeyer, and J. R. Horner. 2005. Gender-specific reproductive tissue in ratites and *Tyrannosaurus rex*. Science 308:1456–1460.

Shine, R., and E. L. Charnov. 1992. Patterns of survival, growth, and maturation in snakes and lizards. American Naturalist 139:1257–1269.

Varricchio, D. J. 2011. A distinct dinosaur life history? Historical Biology 23:91–107.

Varricchio, D. J., J. R. Moore, G. M. Erickson, M. A. Norell, F. D. Jackson, and J. J. Borkowski. 2008. Avian paternal care had dinosaur origin. Science 322:1826–1828.

Wang, S., J. Stiegler, R. Amiot, X. Wang, G.-H. Du, J. M. Clark, and X. Xu. 2017. Extreme ontogenetic changes in a ceratosaurian theropod. Current Biology 27:144–148.

Warshaw, J. 2008. Comparative primate bone microstructure: records of life history, function, and phylogeny; pp. 385–425 in E. J. Sargis and M. Dagosto (eds.), Mammalian Evolutionary Morphology: A Tribute to Frederick S. Szalay. Springer, Dordrecht, The Netherlands.

Werning, S. 2012. The ontogenetic osteohistology of *Tenontosaurus tilletti*. PLoS ONE 7:e33539.

Woodward, H., K. Padian, and A. H. Lee. 2013. Skeletochronology; pp. 195–215 in K. Padian and E.-T. Lamm (eds.), Bone Histology of Fossil Tetrapods: Advancing Methods, Analysis, and Interpretation. University of California Press, Berkeley, California.

Woodward, H. N., E. A. F. Fowler, J. O. Farlow, and J. R. Horner. 2015. *Maiasaura*, a model organism for extinct vertebrate population biology: a large sample statistical assessment of growth dynamics and survivorship. Paleobiology 41:503–527.

Woodward, H. N., T. H. Rich, A. Chinsamy, and P. Vickers-Rich. 2011. Growth dynamics of Australia's polar dinosaurs. PLoS ONE 6: e23339.

Xu, X., X.-L. Wang, and H.-L. You. 2000. A primitive ornithopod from the Early Cretaceous Yixian Formation of Liaoning. Vertebrata PalAsiatica 38:318–325.

Zhao, Q., M. J. Benton, S. Hayashi, and X. Xu. 2019. Ontogenetic stages of ceratopsian dinosaur *Psittacosaurus* in bone histology. Acta Palaeontologica Polonica 64:323–334.

Zhao, Q., M. J. Benton, X. Xu, and P. M. Sander. 2014. Juvenile-only clusters and behaviour of the Early Cretaceous dinosaur *Psittacosaurus*. Acta Palaeontologica Polonica 59:827–833.

Zhao, Q., M. J. Benton, C. Sullivan, P. M. Sander, and X. Xu. 2013. Histology and postural change during the growth of the ceratopsian dinosaur *Psittacosaurus lujiatunensis*. Nature Communications 4:2079.

Zug, G. R., and A. H. Wynn. 1986. Age determination of loggerhead sea turtle, *Caretta caretta*, by incremental growth marks in the skeleton. Smithsonian Contributions of Zoology 427:1–34.